Neurobiology of Disease 130 (2019) 104513

Contents lists available at ScienceDirect

Neurobiology of Disease

journal homepage: www.elsevier.com/locate/ynbdi

Viral delivery of a microRNA to *Gba* to the mouse central nervous system models neuronopathic Gaucher disease

Kasey L. Jackson[a,1], Catherine Viel[a,1], Jennifer Clarke[a], Jie Bu[a], Monyrath Chan[a], Bing Wang[b], Lamya S. Shihabuddin[a], S. Pablo Sardi[a,*]

[a] Rare and Neurologic Diseases Research Therapeutic Area, Sanofi, Framingham, MA 01701, United States of America
[b] Analytical R&D, Sanofi, Waltham, MA 02451, United States of America

ARTICLE INFO

Keywords:
Neuronopathic Gaucher disease
Gba
Ataxia
AAV-mediated microRNA reduction

ABSTRACT

Pathological mutations in *GBA,* encoding lysosomal glucocerebrosidase (GCase), cause Gaucher disease (GD). GD is a multi-system disease with great phenotypic variation between individuals. It has been classified into type 1 with primarily peripheral involvement and types 2 and 3 with varying degrees of neurological involvement. GD is characterized by decreased GCase activity and subsequent accumulation of its lipid substrates, glucosylceramide and glucosylsphingosine. Current murine models of neuronopathic GD mostly replicate the severe aspects of the neurological symptoms developing rapid progression and early lethality, thus presenting a short window for therapeutic testing. In order to develop a model of chronic neuronopathic GD, we reduced GCase in the central nervous system (CNS) of a mild GD mouse model ($Gba^{D409V/D409V}$) via intracerebroventricular administration of an adeno-associated virus encoding a microRNA to *Gba* (AAV-GFP-miR-*Gba*). $Gba^{D409V/D409V}$ mice have significantly reduced GCase activity and increased substrate accumulation in the CNS. Phenotypically, these mice partially recapitulate features of mild type 1 GD. Their neurological examination reveals cognitive impairment with normal motor features. Administration of AAV-GFP-miR-*Gba* into $Gba^{D409V/D409V}$ pups in the CNS caused progressive lipid substrate accumulation. Phenotypically, AAV1-GFP-miR-*Gba*-treated mice were indistinguishable from their littermates until 10 weeks of age, when they started developing progressive neurological impairments, including hyperactivity, abnormal gait, and head retroflexion. Importantly, these impairments can be prevented by simultaneous administration of a miR-resistant *GBA*, demonstrating that the pathological effects are specifically due to *Gba* mRNA reduction. This novel model of neuronopathic GD offers several advantages over current models including slower progression of neurological complications and an increased lifespan, which make it more amenable for therapeutic testing.

1. Introduction

Gaucher disease (GD) is a rare lysosomal storage disease caused by homozygous or compound heterozygous mutations in the *GBA* gene. *GBA* encodes the lysosomal enzyme glucocerebrosidase (GCase), which catabolizes the glycosphingolipids, glucosylceramide (GlcCer) and glucosylsphingosine (GlcSph). The presence of pathological mutations in *GBA* significantly reduces the enzymatic activity of GCase and perturbs associated glycosphingolipid pathways, resulting in the accumulation of undegraded GlcCer and GlcSph in skeletal and visceral tissues and in the central nervous system (CNS) (Orvisky et al., 2000, 2002; Grabowski, 2008).

GD is divided into three clinical subtypes based on the presence or absence of neurological involvement and the rate of disease progression (Grabowski, 2008; Roshan Lal and Sidransky, 2017). Type 1 GD develops primarily peripheral pathology and patients are at an increased risk of developing Parkinson's disease and dementia with Lewy bodies. Type 2 GD progresses rapidly with severe neurological symptoms and death typically by age 2. Type 3 GD has an increased life expectancy compared to type 2 and a slower progression of neurological

Abbreviations: 4-MU, 4-methylumbelliferyl-β-d-glucopyranoside; AAV, adeno-associated virus; ANOVA, analysis of variance; CNS, central nervous system; DAPI, 4′, 6-diamino-2-phenylindole; DMEM, Dulbecco's modified Eagle's medium; Drp, DNase-resistant particle; GCase, glucocerebrosidase; GD, Gaucher disease; GFP, green fluorescent protein; GlcCer, glucosylceramide; GlcSph, glucosylsphingosine; ICV, intracerebroventricular; miR, microRNA; P0, day of birth; PBS, phosphate-buffered saline; RT-qPCR, reverse transcriptase quantitative polymerase chain reaction; TLDA, TaqMan low density array

* Corresponding author at: 49 New York Ave, Framingham, MA 01701, United States of America.
E-mail address: pablo.sardi@sanofi.com (S.P. Sardi).

[1] These authors contributed equally to this manuscript.

https://doi.org/10.1016/j.nbd.2019.104513
Received 1 February 2019; Received in revised form 3 June 2019
Available online 21 June 2019

impairments, including ataxia and tremor. Neuronopathic GD (types 2 and 3) is particularly challenging to treat as the currently approved therapies are not brain penetrant or have no effect on neurological symptoms (Grabowski, 2008; Roshan Lal and Sidransky, 2017; Shawky and Elsayed, 2016). Although many murine models are invaluable in regards to understanding the underlying disease mechanisms involved in GD, they present an extremely limited window for therapeutic intervention and/or do not recapitulate the disease course seen in patients with type 3 GD (Farfel-Becker et al., 2011; Sanders et al., 2013).

Several murine models of GD have been used preclinically to test the efficacy of disease-modifying therapeutics and therapeutic approaches (Sardi et al., 2013; Mistry et al., 2014; Dahl et al., 2015; Marshall et al., 2016; Marshall et al., 2010). The neuronopathic GD models exhibit very minimal residual GCase activity (e.g. $Gba^{-/-}$ animals have GCase activity of < 4% that of wild-type animals), and thus have severe early-onset neurological abnormalities and early mortality (Farfel-Becker et al., 2011), a similar disease course to that of type 2 GD patients. On the contrary, mouse models of non-neuronopathic type 1 GD have adult-onset disease pathology and lack many of the severe neurological phenotypes (Farfel-Becker et al., 2011). In order to address the need for a model reflective of type 3 GD, we hypothesized that reducing the expression of endogenous GCase in the CNS of a non-neuronopathic, type 1, model of GD ($Gba^{D409V/D409V}$ transgenic mouse) (Xu et al., 2003) would provoke neurological dysfunction and allow for a more protracted disease course amenable to therapeutic testing. Here, we used an adeno-associated virus (AAV) to express a micro-RNA (miR) against the endogenous mouse *Gba* in $Gba^{D409V/D409V}$ mice and evaluated glycosphingolipid accumulation, inflammation, and behavior.

2. Materials and methods

2.1. Plasmids and AAV vectors

The plasmids used to generate AAV2/1-GusB-GFP or AAV2/1-GusB-*GBA* allow for the expression of GFP or human *GBA* and have been previously described (Sardi et al., 2011). To examine the long-term effects of glucocerebrosidase knockdown in the brain, an artificial micro-RNA (miR)-based hairpin against mouse *Gba* was inserted to generate AAV2/1-GusB-GFP-miR-*Gba* (TATACCAGTGAACAGCAATGC CGTTTTGGCCACTGACTGAC**GGCATTGCTTCACTGGTATA**CAGGACAC AAGG, bolded = *Gba* targeting sequence). Preliminary experiments showed that this miR sequence was also able to partially knockdown human *GBA*. Thus, a series of synonymous mutations were introduced to the human *GBA* coding sequence to generate AAV2/1-GusB-*GBA**-miR-*Gba*, where *GBA** is resistant to the artificial miR (Fig. S1). The recombinant plasmids were each packaged into AAV serotype-1 capsids by triple-plasmid transfection of human HEK293 cells to generate AAV2/1-GusB-GFP (AAV1-GFP), AAV2/1-GusB-GFP-miR-*Gba* (AAV1-GFP-miR-*Gba*), and AAV2/1-GusB-*GBA**-miR-*Gba* (AAV1-*GBA**-miR-*Gba*). Recombinant AAV vectors were purified by ion-exchange chromatography. The resulting vector preparations typically possessed titers of 1e13 DNase-resistant particles (drp)/mL (Sardi et al., 2011).

2.2. Cell culture and infection

Mouse embryonic fibroblast cells (NIH-3T3) were infected with either AAV1-GFP or AAV1-GFP-miR-*Gba* (5 to 10 e6 multiplicity of infection) which allowed 100% infection efficiency. Cells were co-infected with adenovirus Ad-TS as a helper virus for increased expression and harvested 48 or 96 hours post-infection for mRNA or protein analysis, respectively.

2.3. Animals

All procedures were performed according to a protocol approved by the Institutional Animal Care and Use Committee at Sanofi. $Gba^{D409V/D409V}$ mice, which harbor a point mutation at residue 409 in the murine glucocerebrosidase (*Gba*) gene (Xu et al., 2003) on a C57Bl/6 background, and C57Bl/6 WT mice were utilized. Animals were group housed under 12-hour light:dark cycles and provided with food and water ad libitum. All behavioral testing was performed during the animals' light cycle, between the hours of 8 AM and 4 PM.

2.4. Neonatal injections

On the day of birth (P0), pups received bilateral intracerebroventricular (ICV) injections (2 μL at each site). The total dose of AAV1-GFP, AAV1-*GBA**-miR-*Gba*, and AAV1-GFP-miR-*Gba* vectors administered was 4e10 DNase-resistant particles (drp) per animal. All injections were performed with finely drawn glass micropipette needles as previously described (Snyder et al., 1995; Passini et al., 2011).

2.5. Animal perfusion and tissue collection

Animals were transcardially perfused with cold phosphate-buffered saline (PBS). The brains were cut sagittally along the midline. The left hemisphere was dissected into various regions, snap-frozen in liquid nitrogen, and stored at −80 °C until use. The right hemisphere was post-fixed in 10% neutral-buffered formalin for 48 h before being washed three times in PBS and transferred to 30% sucrose. Right hemispheres were embedded in OCT and sectioned into 20 μm sections using a cryostat.

2.6. Flow cytometry analysis

Liver, brain and spinal cord were isolated from AAV1-GFP-miR-*Gba* injected mice perfused with phosphate-buffered saline (PBS) before being digested with a Dulbecco's modified Eagle's medium (DMEM)-Papain solution for 30 min in a 37 °C water bath. Cells were dissociated via gentle pipetting and centrifuged at 3000 RPM for 5 min at 4 °C. Cells were resuspended in DMEM supplemented with 10% fetal bovine serum and filtered through a 40 μm cell strainer on ice. GFP-positive samples were acquired using an LSRII flow cytometer (BD Biosciences, San Jose, CA) and data were analyzed using FLOWJO software v.7–6-5 (Tree Star, Ashland, OR). The live gate was used to select the cells for analysis. Propidium iodide was used to determine live cells.

2.7. Measurements of glucocerebrosidase activity and glycosphingolipid levels

Tissue levels of glucosylceramide (GlcCer) and glucosylsphingosine (GlcSph) were measured by liquid chromatography and tandem mass spectrometry (LC-MS/MS) as previously described (Sardi et al., 2013). Briefly, brain tissue homogenates were extracted with 1 mL of an organic solvent mixture. The extracted sphingolipids (GlcCer and GlcSph) were directly separated by hydrophilic liquid chromatography (Atlantis and BEH Hilic columns, respectively; Waters), analyzed by triple quadrupole tandem mass spectrometry (API 5000, Applied Biosystems/MDS SCIEX; and Agilent 6490, Agilent Technologies, respectively), and compared with sphingolipid standards (Matreya, Pleasant Gap, PA). Brain glucocerebrosidase activities were determined as previously described using 4-methylumbelliferyl-β-d-glucopyranoside (4-MU) as the artificial substrate (Sardi et al., 2013).

2.8. Immunohistochemistry and morphometric analysis

All brain sections were blocked with 10% (vol/vol) serum for 1 h at room temperature and incubated with anti-GFAP (1:2500 dilution; DAKO, Santa Clara, CA), anti-Iba1, or anti-NeuN overnight at 4 °C. Brain sections were then incubated for 1 h with donkey anti-rabbit Alexa Fluor-555 secondary antibody (1:250 dilution; Invitrogen, Carlsbad, CA). Cell nuclei were stained with DAPI (Sigma-Aldrich).

Sections were coverslipped with aqua-poly/mount (Polysciences, Warrington, PA) and the cerebellum and cortex were imaged with a SPOT camera (SPOT Imaging, Sterling Heights, MI) paired with a Nikon Eclipse E800 fluorescence microscope equipped with a 20× objective lens. Two to three sections were imaged per animal, and GFAP immunofluorescence was quantitatively measured via threshold fluorescent area on MetaMorph Software (Molecular Devices, San Jose, CA). These procedures were performed blinded to the genotype or treatment.

2.9. Open field

General locomotor activity was assessed at 30 weeks of age. Briefly, animals were placed in a Plexiglas cage and allowed to move freely for 30 min. A photobeam array was placed around the exterior of the cage to record the animals' movements as successive beam breaks (Open Field Activity System; Med Associates, Fairfax, VT). Total distance traveled (ambulatory distance) and total time spent traveling (ambulatory time) were calculated to assess general motor activity.

2.10. Accelerating rotarod test

Motor coordination was assessed on an accelerating rotarod apparatus (Ugo Basile, Varese, Italy). Mice were trained on the rotarod with three trials per day for two consecutive days. On the first training day, the rotarod was set at a constant speed of 5 RPM over 120 s. Mice that fell off the rod before completion of the 120-sec time period were placed back on the rod until the full 120-sec period had elapsed. On the second day of training, the rotarod was set to accelerate from 5 to 40 RPM over 300 s. Animals were not replaced after falling. On the third day (test day), the mice were placed on the rotarod set to accelerate from 5 to 40 RPM over 300 s. Animals were not replaced after falling, and the latency to fall was recorded over three trials. The average latency to fall of the three trials was used for analyses.

2.11. Gait and hyperactivity evaluation

Gait and hyperactivity were qualitatively measured at 6 week intervals for all animals. A clinical score of 0, 1, or 2 (normal, symptomatic, or end stage, respectively) was assigned based on individual phenotypic observations over a 1 minute trial in a new housing cage with cob bedding and no enrichment.

Gait: A score of 0 (normal) was assigned if the animal exhibited a normal, stable gait phenotype with their hind limbs and paws facing in a near-forward direction (near-parallel to the mid line of the body) when moving while maintaining their balance. A score of 1 (symptomatic) was assigned to an animal with abnormal placement of the hind limbs and paws (near-perpendicular to the mid line of the body), elongated distance between steps, and difficulty balancing while moving. A score of 2 (end stage) was given to an animal with a severe, unstable gait phenotype featuring abnormal placement of the hind limbs and paws (perpendicular to the mid line of the body), an elongated distance between steps, and general inability to maintain their balance.

Hyperactivity: A score of 0 (normal) was assigned if the animal exhibited typical activity levels characterized by periods of rest and ambulation during the 1 minute trial, along with the absence of hyperactivity and circling behaviors. A score of 1 (symptomatic) was assigned if the animal exhibited mild hyperactivity characterized by some circling behavior and an increase in periods of ambulation and less rest. A score of 2 (end stage) was given to an animal if they exhibited severe hyperactivity during the 1 minute trial, characterized by unrelenting circling behavior along with a significant increase in periods of ambulation with no rest.

2.12. Head retroflexion (neck hyperextension) quantification

Head retroflexion was evaluated at 6 week intervals for each animal by recording the number of head-tossing events over a 1 minute trial. A head-tossing, or retroflexion, event was defined as the position of the animal's nose rapidly moving from a neutral position (nose position is in-line with the spinal column) upward by 70–90° (nose position is perpendicular to the spinal column).

2.13. Reverse transcriptase quantitative PCR (RT-qPCR) and TaqMan Low Density Array (TLDA)

Mouse cortical mRNA levels were measured via RT-qPCR and TLDA. NIH-3T3 cell mRNA was quantified by RT-qPCR. Briefly, total RNA was extracted using an RNeasy mini kit (Qiagen, Valencia, CA) and reverse transcribed and amplified with a TaqMan One-Step RT-PCR master mix kit (Life Technologies, Carlsbad, CA), according to the manufacturer's instructions.

RT-qPCR: Relative mRNA levels of the target genes were measured and analyzed on an ABI Prism 7500 (Life Technologies, CA). The expression levels of mouse *Gba* (Mm00484700_m1) and *Gba2* (Mm00554547_m1) mRNA were normalized to mouse hypoxanthine-guanine phosphoribosyltransferase-1 (*Hprt*). Standard curves were generated using 5-fold serial dilutions of pooled mouse cortical cDNA or cell cDNA. Samples were run in duplicate and relative gene expression was interpolated from a standard curve.

TLDA: Relative mRNA levels of target genes were measured via RT-qPCR using a microfluidic card, TLDA, on an ABI Prism 7500 (Life Technologies, CA), and gene expression levels were normalized using DataAssist v2.0 Software (Life Technologies, CA). Endogenous controls used for the analysis were mouse peptidyl-prolyl cis-trans isomerase A (*Ppia*), *Hprt*, and β-actin mRNAs.

2.14. Statistical analysis

Parametric statistical analyses were performed by Student's *t*-test or analysis of variance (ANOVA) followed by Tukey's post-hoc analysis. Nonparametric data were analyzed by Kruskal-Wallis test with Dunn's multiple comparison analysis. All statistical analyses were performed using GraphPad Prism v4.0 (GraphPad Software, San Diego, CA). A p-value of < 0.05 was considered a statistically significant difference.

3. Results

3.1. AAV1-GFP-miR-Gba administration reduces Gba mRNA and GCase activity in vitro

Virus specificity and *Gba* knockdown were confirmed in mouse NIH-3T3 cells. Mouse *Gba* mRNA was significantly reduced (~80% reduction) while non-lysosomal, mouse *Gba2* mRNA remained unchanged in cells treated with either AAV1-GFP-miR-*Gba* or AAV1-*GBA**-miR-*Gba* (Fig. 1A, C). The AAV1-*GBA**-miR-*Gba* contains a mutant human *GBA* sequence that is not recognized by the mouse-specific primers for *Gba* mRNA. Accordingly, lysosomal GCase activity was also reduced whereas non-lysosomal (*Gba2*-related) GCase activity remained the same in AAV1-GFP-miR-*Gba* infected cells (Fig. 1B, D). Conversely, both lysosomal and non-lysosomal GCase activity were unchanged in AAV1-*GBA**-miR-*Gba* infected cells, as AAV1-mediated overexpression of the miR-resistant human *GBA* maintains GCase activity comparable to non-transfected and GFP expressing cells despite knockdown of endogenous mouse *Gba*. These results confirm the knockdown specificity and protein expression of the AAVs used in these studies.

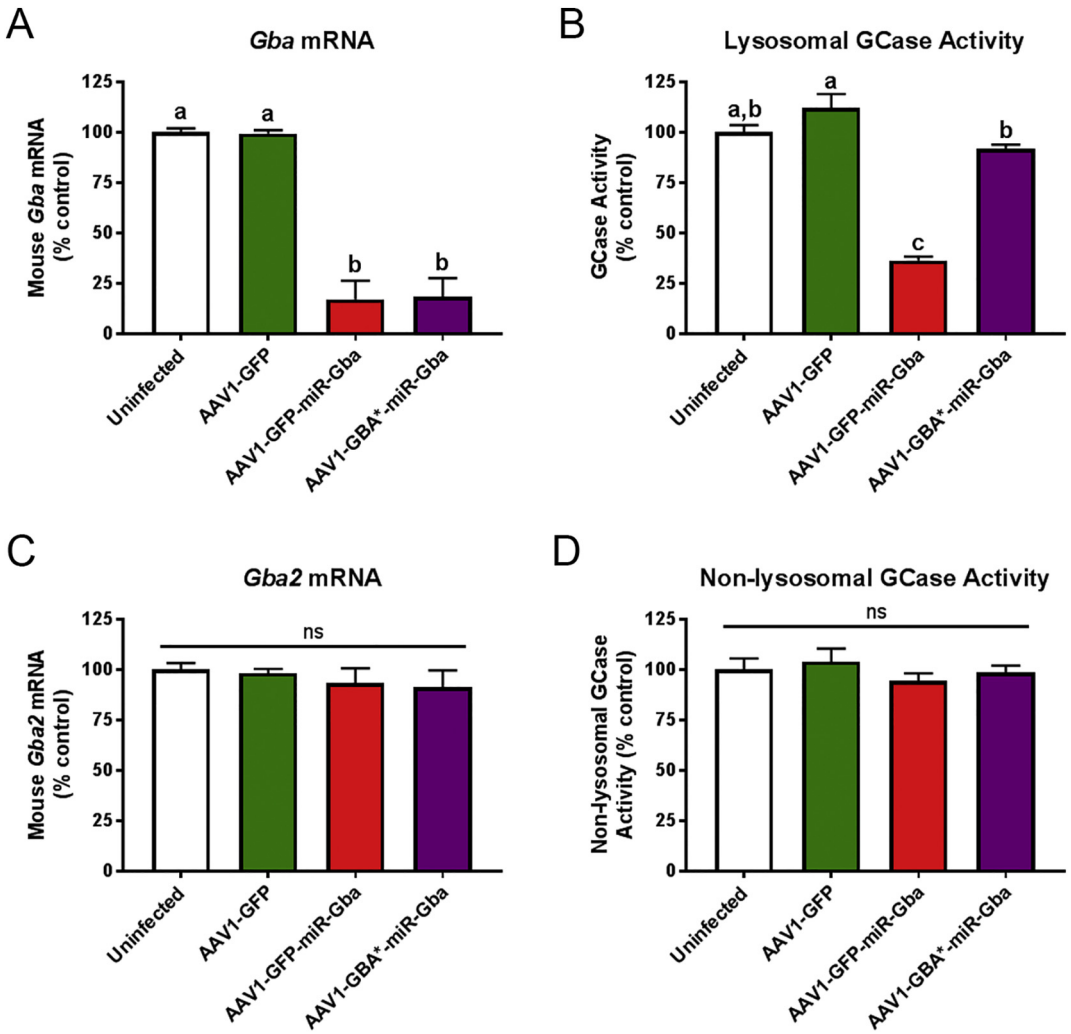

Fig. 1. AAV1-GFP-miR-*Gba* selectively knocks down murine *Gba* mRNA levels and decreases lysosomal GCase activity in vitro. Mouse NIH-3T3 cells were infected with AAVs expressing GFP, GFP-miR-*Gba*, or *GBA**-miR-*Gba* (*GBA**: miR-resistant *GBA*). (A) Endogenous mouse *Gba* mRNA was significantly decreased in both groups expressing miR-*Gba*. (B) Lysosomal GCase activity was significantly reduced in the AAV1-GFP-miR-*Gba* group and rescued by AAV1-*GBA**-miR-*Gba*. (C, D) *Gba2* mRNA levels and non-lysosomal GCase activity were not affected by any of the treatments. One-way ANOVA with Tukey's post-hoc analysis. Bars with different letters are significantly different from each other ($p < 0.05$). $N = 3$/group.

3.2. AAV1-GFP-miR-Gba administration broadly transduces neurons in vivo and significantly reduces Gba mRNA

To determine the extent of viral transduction and expression after P0 ICV injections, a subset of AAV1-GFP-miR-*Gba*-injected animals were sacrificed 6 weeks post-injection and evaluated by flow cytometry and fluorescence microscopy. Evaluation of the percentage of GFP-positive cells in various regions of the CNS showed high percentages of transduced cells in the cortex, hippocampus, striatum, and thalamus, and lower percentages in the brain stem, cerebellum, and spinal cord (Fig. 2A). Histological analysis of GFP expression at 6 months post-injection in a subset of animals also supported this observation (Fig. 2B–D). The primary cell type transduced was neurons in the CNS (Fig. 2B–D); no GFP-positive microglia or astrocytes were observed following AAV1-GFP-miR-*Gba* administration (Fig. S2).

The effect of these vectors was also tested in vivo by quantifying *Gba* mRNA knockdown and lysosomal glucocerebrosidase activity after P0 ICV injections in $Gba^{D409V/D409V}$ mice. Administration of AAV1-GFP-miR-*Gba* significantly decreased *Gba* mRNA in the cortex of the mutant mice compared to AAV1-GFP injected littermates (Fig. 3A) and did not affect *Gba2* mRNA levels (Fig. 3B). $Gba^{D409V/D409V}$ transgenic mice retain approximately 25% GCase activity in the CNS compared to wild-type controls (Xu et al., 2003). No decrease in cortical GCase activity was found in AAV1-GFP-miR-*Gba*-injected brains, possibly due to a floor effect in the 4-MU assay and/or a dilution effect due to incomplete transduction (~40% of cells were not transduced in the cortex). Importantly, GCase activity was considerably increased in the cortex by the rescue vector (AAV1-*GBA**-miR-*Gba*; Fig. 3C), confirming the expression of the miR-resistant human *GBA* transgene.

3.3. AAV1-GFP-miR-Gba treatment promotes additional substrate accumulation in the CNS of $Gba^{D409V/D409V}$ mice

$Gba^{D409V/D409V}$ mice preferentially accumulate GlcSph as opposed to GlcCer in the CNS (Xu et al., 2003). To evaluate the effects of knocking down endogenous mouse GCase activity on the glycosphingolipid pathway, GlcCer and GlcSph were quantified in the cortex and the cerebellum. Administration of AAV1-GFP-miR-*Gba* into newborn $Gba^{D409V/D409V}$ mice promoted a significant increase in GlcSph in the cortex (Fig. 3D) and cerebellum (Fig. S3A) at 30 weeks of age, suggesting perturbation of glycosphingolipids and reduced GCase activity. Interestingly, AAV1-GFP-miR-*Gba*-treated animals displayed GlcCer accumulation in the cerebellum (Fig. S3B) but not the cortex (Fig. 3E), indicating a differential regional susceptibility to miR-mediated GCase

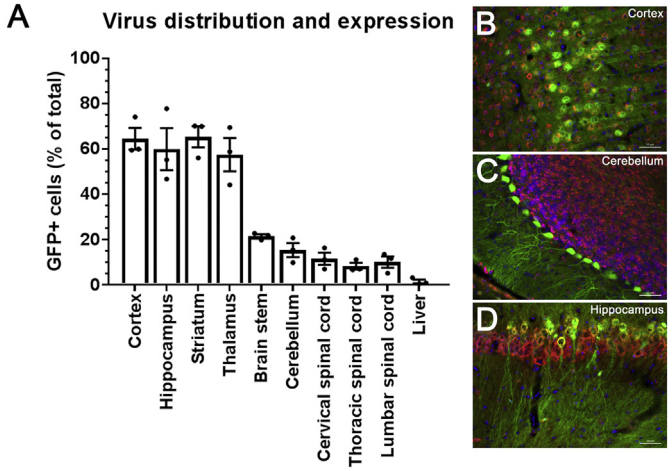

Fig. 2. AAV1 shows widespread transduction of cells throughout the CNS after neonatal ICV injection. (A) Percentage of GFP-expressing cells in various CNS regions and liver. GFP (green) and NeuN (red) expression in the (B) cortex, (C) cerebellum, and (D) hippocampus. Scale bar is 50 μm; 20× magnification in all images. (For interpretation of the references to colour in this figure legend, the reader is referred to the web version of this article.)

reduction.

As anticipated, administration of AAV1-*GBA**-miR-*Gba* increased GCase activity (Fig. 3C) and prevented the buildup of glycosphingolipid substrate in cortex and cerebellum (Fig. 3D, and Fig. S3A, B). These data support our hypothesis that further reducing endogenous mouse GCase activity in $Gba^{D409V/D409V}$ mice exacerbates the disruption of the glycosphingolipid pathway and confirms the specificity of the AAV1-GFP-miR-*Gba* construct.

3.4. Administration of AAV1-GFP-miR-Gba in $Gba^{D409V/D409V}$ mice induces progressive hyperactivity and ataxia

Previous phenotypic characterization of the $Gba^{D409V/D409V}$ mouse model by our group revealed cognitive impairment without motor dysfunction (Sardi et al., 2011). Preliminary evaluation of AAV1-GFP-miR-*Gba*-treated $Gba^{D409V/D409V}$ and WT animals suggested the presence of motor abnormalities only in mutant animals (Fig. S4) and prompted the systematic and careful characterization of the motor phenotypes in longitudinal cohorts of $Gba^{D409V/D409V}$ mice (Fig. S5, S6). Littermates were either left untreated or ICV-injected at P0 with AAV1-GFP, AAV1-GFP-miR-*Gba,* or AAV1-*GBA**-miR-*Gba.* Animals were evaluated for hyperactivity, gait, rotarod performance, and head retroflexion every 6 weeks from 6 to 30 weeks of age and evaluated for general activity using the open field activity test at 30 weeks of age (Fig. 4A). All groups were phenotypically indistinguishable up to 10 weeks of age, when some animals began to display increased movement. Mice administered AAV1-GFP-miR-*Gba* showed increasingly higher hyperactivity scores, with significant increases at 18, 24, and 30 weeks (Fig. 4C). This hyperactivity phenotype was further confirmed and objectively quantified using the open field activity test at 30 weeks of age, where total ambulatory-time and -distance traveled were significantly increased in animals administered AAV1-GFP-miR-*Gba* (Fig. 4D, E). Increases in hyperactivity score and total ambulatory time and distance were prevented by overexpression of miR-resistant *GBA* in the context of endogenous *Gba* knockdown (Fig. 4C–E; Video S1), confirming the specificity of the miR-mediated GCase reduction.

Accompanying the hyperactivity in these animals was a propensity for head retroflexion and gait abnormalities. The frequency of head retroflexions progressively increased from 18 to 30 weeks of age and was only detected in animals administered AAV1-GFP-miR-*Gba* (Fig. 4F). Gait abnormalities, including abnormal placement of the

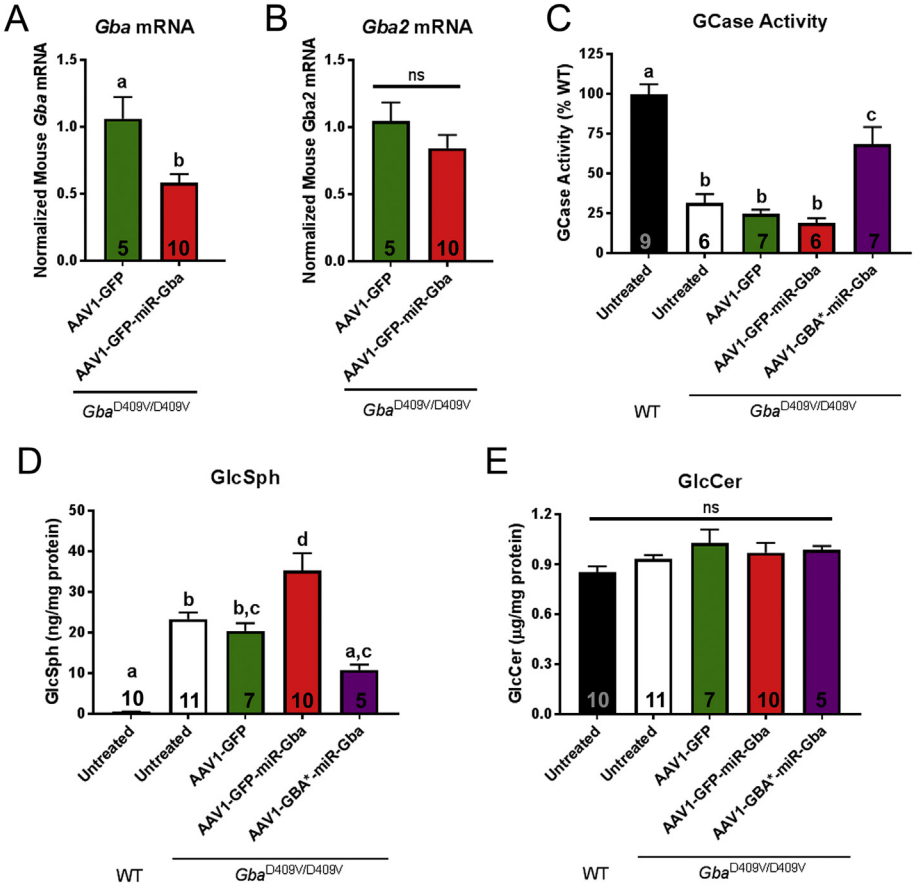

Fig. 3. miR-*Gba* expression in $Gba^{D409V/D409V}$ mouse brain decreases *Gba* mRNA and increases GlcSph in the cortex. (A) Administration of AAV1-GFP-miR-*Gba* at P0 reduced murine *Gba* mRNA in the cortex compared to AAV1-GFP. (B) These treatments caused no changes in *Gba2* mRNA levels. (C) Cortical GCase activity is significantly decreased in $Gba^{D409V/D409V}$ animals and no further reduction is realized with the administration of AAV1-GFP-miR-*Gba.* Treatment with AAV1-*GBA**-miR-*Gba* reinstates the enzymatic activity. (D) GlcSph was significantly increased by AAV1-GFP-miR-*Gba* compared to AAV1-GFP or untreated $Gba^{D409V/D409V}$ animals. The GlcSph accumulation was prevented by AAV1-*GBA**-miR-*Gba*. (E) None of these treatments affect GlcCer substrate levels in the cortex of mutant or wild-type mice. (A, B) Student's *t*-test. (C-E) One-way ANOVA followed by Tukey's post-hoc analysis. Bars with different letters are significantly different from each other ($p < 0.05$). $N = 5–11$/group.

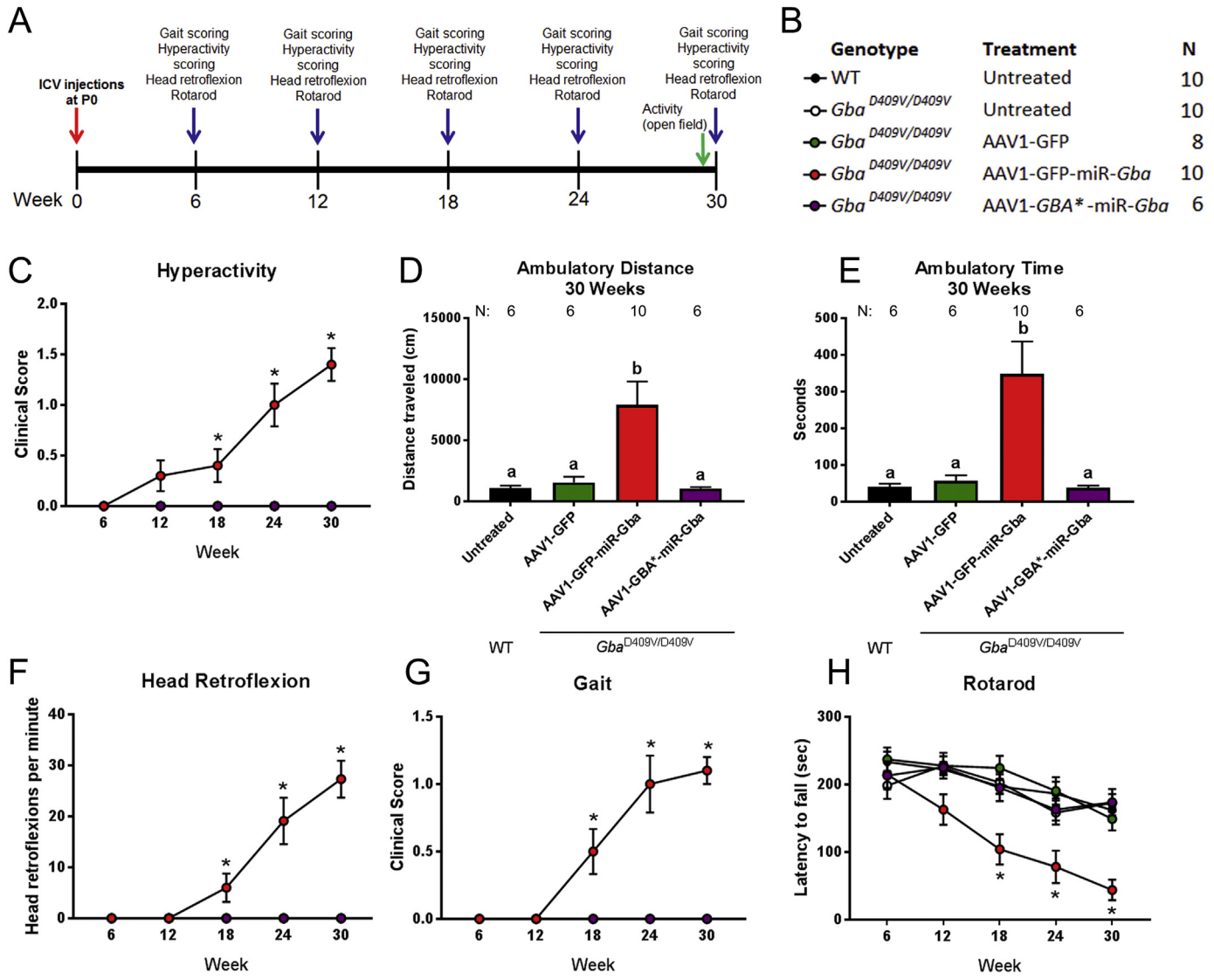

Fig. 4. AAV1-GFP-miR-*Gba* administration causes progressive motor deficits and hyperactivity. (A) Timeline of behavioral activities. (B) Group descriptions with N values for graphs C and F–H. N values for D and E noted on the graphs. (C) Hyperactivity scores in mice administered AAV1-GFP-miR-*Gba* progressively increased from 6 to 30 weeks of age. Hyperactivity was not observed in any of the other groups tested. (D–E) The hyperactive phenotype was confirmed via an open field activity chamber at 30 weeks of age where the AAV1-GFP-miR-*Gba* group displayed increased ambulatory distance and ambulatory time. (F) Mice administered AAV1-GFP-miR-*Gba* displayed head retroflexion which increased in frequency from 12 to 30 weeks of age (see Video S1). (G) The AAV1-GFP-miR-*Gba* group also displayed impairments in gait which were significantly different from 18 to 30 weeks of age (see Video S1). (H) Performance on the rotarod was significantly impaired in the AAV1-GFP-miR-*Gba* group by 18 weeks of age and further declined to 30 weeks of age. (C, G) Kruskal-Wallis test followed by Dunn's multiple comparisons test. (D, E) One-way ANOVA followed by Tukey's post-hoc analysis. (F, H) Two-way RM-ANOVA followed by Tukey's post-hoc analysis. Bars with different letters are significantly different from each other ($p < 0.05$).

hindpaws when walking and general imbalance, were only seen in animals administered AAV1-GFP-miR-*Gba,* beginning between weeks 12 and 18 and progressively increasing in severity up to 30 weeks of age (Fig. 4G).

The mice were also evaluated for motor dysfunction via accelerating rotarod (Fig. 4H). There was no difference between wild-type animals and untreated or AAV1-GFP-injected $Gba^{D409V/D409V}$ mice. However, motor function progressively declined in animals administered AAV1-GFP-miR-*Gba* and was significantly decreased compared to wild-type animals from 18 to 30 weeks of age. Remarkably, administration of AAV1-*GBA**-miR-*Gba* successfully prevented this decline in motor function.

3.5. Administration of miR-Gba in $Gba^{D409V/D409V}$ mice promotes astrogliosis

$Gba^{D409V/D409V}$ mice display no evidence of neuroinflammation compared to wild-type animals (Sardi et al., 2011). GFAP, an astrocyte marker whose expression is increased with astrogliosis, was evaluated in the cortex and cerebellum via immunofluorescence and TLDA analysis. As previously reported by our group (Sardi et al., 2011), there was no increase in GFAP immunostaining between wild-type and $Gba^{D409V/D409V}$ mice. However, mice administered AAV1-GFP-miR-*Gba* displayed a significant increase in GFAP immunoreactivity by immunofluorescent staining in the cerebellum (Fig. 5A). A trend toward an increase in GFAP immunoreactivity ($p = 0.08$) was also observed in the cortex of mice administered AAV1-GFP-miR-*Gba* (Fig. 5B and Fig. S7A). The increased GFAP staining was prevented in the AAV1-*GBA**-miR-*Gba* group in both the cerebellum and cortex. This increase in GFAP

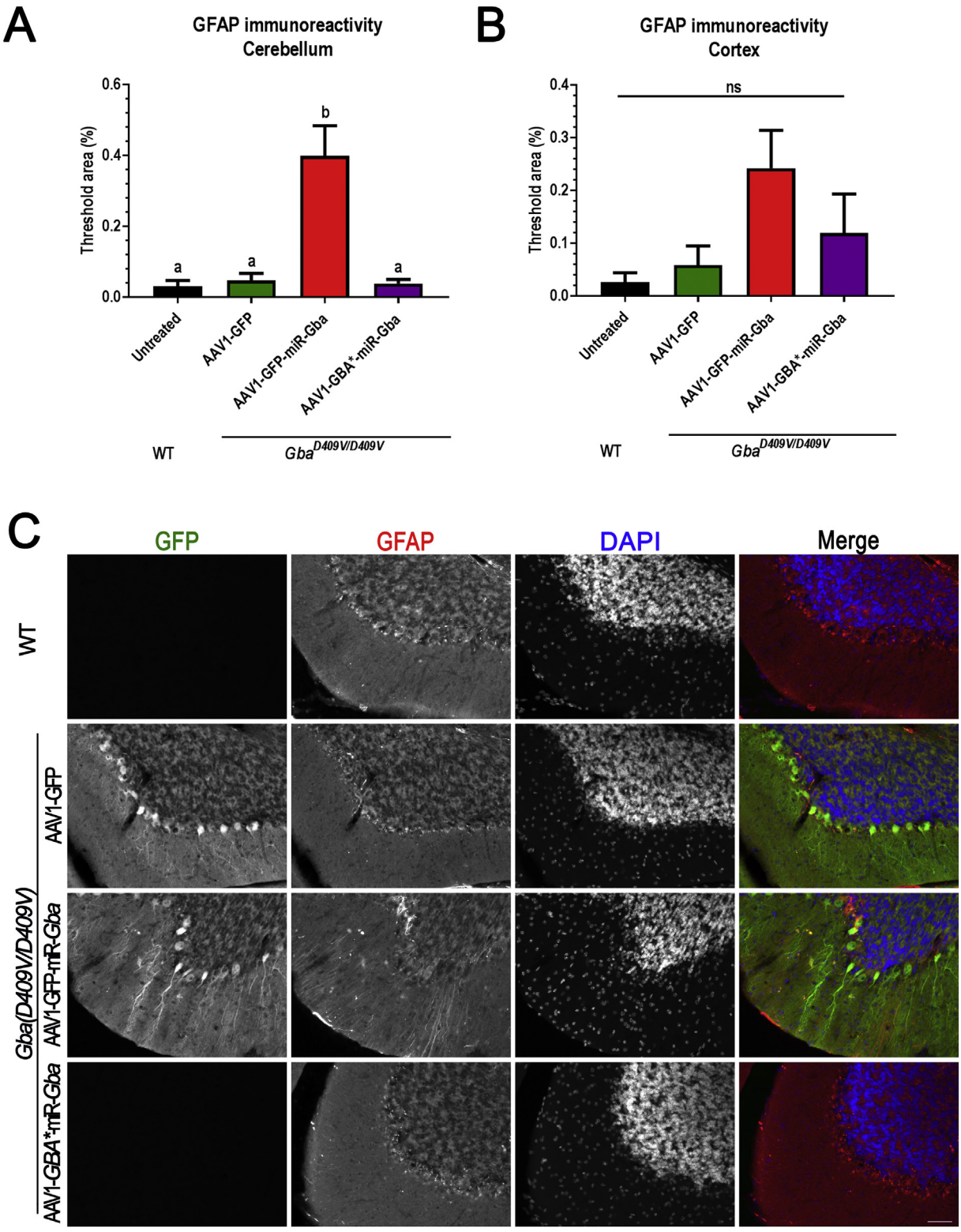

Fig. 5. Increased GFAP immunoreactivity in the cerebellum after AAV1-GFP-miR-*Gba* administration but no effect on IBA1. (A) GFAP immunoreactivity in the cerebellum was significantly increased in the AAV1-GFP-miR-*Gba* group but normal in the AAV1-*GBA**-miR-*Gba* group. (B) No significant increase in GFAP immunoreactivity was observed in the cortex of $Gba^{D409V/D409V}$ animals administered AAV1-GFP-miR-*Gba* ($p = 0.08$). (C) Representative images for GFP (green) and GFAP (red) immunostaining in the cerebellum are shown for WT and $Gba^{D409V/D409V}$ animals administered AAV1-GFP, AAV1-GFP-miR-*Gba*, and AAV1-*GBA**-miR-*Gba*. Scale bar is 50 μm; 20× magnification in all images. One-way ANOVA with Tukey's multiple comparisons test. Differing letters signify statistical difference of $p < 0.05$. $N = 6–7$/group. (For interpretation of the references to colour in this figure legend, the reader is referred to the web version of this article.)

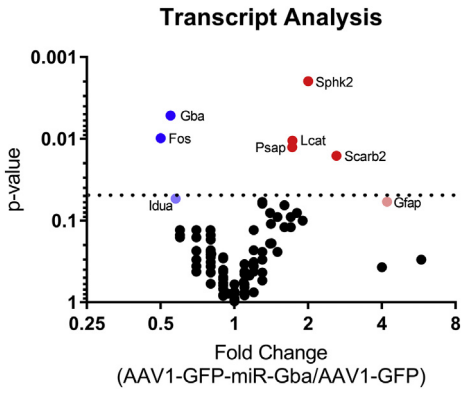

Fig. 6. AAV1-GFP-miR-*Gba* administration causes perturbations in lysosomal function and lipid metabolism in the CNS. The cortices of mice administered either AAV1-GFP or AAV1-GFP-miR-*Gba* through ICV injections at P0 were evaluated for a subset of transcripts involved in neuronal function, lipid metabolism and signaling, and lysosome function via TLDA analysis. A volcano plot depicts the ratio of AAV1-GFP-miR-*Gba* to AAV1-GFP for all transcripts. mRNAs significantly increased in the AAV1-GFP-miR-*Gba* group are shown in red and those decreased are displayed in blue. Light blue and red signify a trend for significance. Dotted line represents $p = 0.05$. Transcripts significantly different between the groups include *Gba*, *Fos, Sphk2, Lcat, Psap,* and *Scarb2*. Additional information provided in Table S1. Student's *t*-test, $N = 5$/AAV1-GFP group and 10/AAV1-GFP-miR-*Gba* group. (For interpretation of the references to colour in this figure legend, the reader is referred to the web version of this article.)

immunoreactivity was also supported by a trend for increased *Gfap* mRNA levels by TLDA in the cortex (4.3-fold increase, $p = 0.059$; Fig. 6 and Table S1).

IBA1, a marker of microglial activation was also evaluated in the cerebellum and cortex via immunofluorescence and TLDA analyses. There was no significant difference in IBA1 immunoreactivity in the cortex (Fig. 7SB) in accordance with the TLDA analysis where *Aif1* was not significantly increased (Fig. 6 and Table S1). Similarly, in the cerebellum, there was no significant difference in IBA1 immunoreactivity between groups (Fig. S7B, C).

3.6. Gene expression alteration in lysosomal function and lipid metabolism

To gain further insights into the molecular mechanisms underlying the behavioral dysfunction associated with decreased glucocerebrosidase levels, we compared the gene expression profiles in the cortex of $Gba^{D409V/D409V}$ mice administered either AAV1-GFP or AAV1-GFP-miR-*Gba*. We evaluated a variety of transcripts involved in neuronal function such as dopaminergic neurotransmission, synaptic function, and calcium homeostasis as well as transcripts involved in lysosomal function and lipid metabolism. Of note, several transcripts involved in lipid metabolism, lipid signaling and lysosomal function were altered between the two groups, including *Lcat*, *Idua*, *Scarb2*, *Psap*, and *Sphk2* (Fig. 6 and Table S1) suggesting more widespread lipid dysregulation.

4. Discussion

The neuronopathic GD patient population has a high unmet medical need as current therapies for GD only address the systemic manifestations of the disease and not the neurological components (Shawky and Elsayed, 2016). Here, we describe a new murine model of neuronopathic GD with progressive neurological dysfunction resembling the human condition and a lifespan amenable to therapeutic intervention.

The $Gba^{D409V/D409V}$ mouse model harbors a homozygous D409V mutation which reduces GCase activity in the liver and brain (< 5% and ~25% of WT, respectively) (Xu et al., 2003). Classical Gaucher cells develop in the spleen beginning around 7 months of age with GlcCer accumulation present in the liver, lung, and spleen (Xu et al., 2003) and progressive GlcSph accumulation in the brain (Sardi et al., 2011). Despite the development of cognitive impairments in this model by 6 months of age (Sardi et al., 2011), the neurological symptoms are subtle and better represent type 1 GD which has a higher risk for the development of Parkinson's disease and dementia with Lewy bodies (Tayebi et al., 2003; Neudorfer et al., 1996; Rosenbloom et al., 2011). In an effort to increase the severity of neurological symptoms similar to those of neuronopathic GD yet maintain an expanded window for therapeutic intervention, we modulated *Gba* in the CNS using a miR within the context of this Type 1 GD mouse model.

Administration of AAV1-GFP-miR-*Gba* to the cerebral ventricles of neonatal $Gba^{D409V/D409V}$ but not wild-type mice resulted in progressive neurological aberrations (head retroflexion and gait abnormalities), hyperactivity, neuroinflammation (astrogliosis), and perturbed lipid metabolism and lysosomal function as shown by TLDA analysis. Importantly, these mice were viable for up to 36 weeks of age. The extended lifespan of these mice as well as the progressive nature of their impairments allows for pre-symptomatic, early stage, and late-symptomatic administration of therapeutics. The pre-symptomatic stage extends into young-adulthood (~10 weeks of age); which, when compared to a neonatal onset, significantly expands the dosing regimens and routes of administration available for therapeutic testing while avoiding the potential complications associated with interfering with early peripheral and neural development. Additionally, the neurological deficits are substantial and can be evaluated using a variety of behavioral paradigms, allowing for easy assessment of improvement or progression of disease and comparisons between therapeutic approaches.

The abnormal behaviors displayed in this mouse model coincide with those observed in neuronopathic GD. Patients with type 3 GD display a variety of neurological problems, including cognitive deficits such as learning disabilities and dementia, motor impairments including ataxia and spasticity, as well as supranuclear gaze palsy and seizures (Roshan Lal and Sidransky, 2017; Abdelwahab et al., 2017). Similarly, administration of AAV1-GFP-miR-*Gba* to $Gba^{D409V/D409V}$ mice caused ataxia. The head retroflexion seen in this model resembles the neck hyperextension observed in type 3 GD, and may be indicative of myoclonic jerks or seizures also seen in type 3 GD (Roshan Lal and Sidransky, 2017; Abdelwahab et al., 2017) or a type of hyperkinetic dystonia as recently described in a subset of patients with type 3 GD (Machaczka et al., 2018). Without the use of EEG monitoring, we could not definitively prove that these mice were having seizures; however, they displayed several behaviors consistent with seizures in rodents (hyperactivity including running fits and circling, head nodding, rearing, and falling) (Pinel and Rovner, 1978). The $Gba^{D409V/D409V}$ mouse model displays cognitive impairment (Sardi et al., 2013); however, the hyperactivity and motor dysfunction that developed after AAV1-GFP-miR-*Gba* administration precluded any behavioral testing to demonstrate additional cognitive impairment.

AAVs are useful for both modeling neurological disorders and evaluating therapeutic targets for diseases of the CNS. The field of neuroscience has exploited many of the natural features of AAVs including the neurotropism of many serotypes, low immunogenicity, low rates of integration, and ability to infect dividing and non-dividing cells (Lentz et al., 2012). However, AAVs do not uniformly affect all cells in the CNS (Hammond et al., 2017), and both modeling and therapeutic targeting may be affected by the route of administration of the AAV as well as the tropism of the selected serotype. The behaviors observed when AAV1-GFP-miR-*Gba* is administered may be due in part to the tropism of the virus and the brain regions which are exposed. AAV1 is known to have a broad distribution after neonatal ICV injection and transduces neurons within the CNS (Passini et al., 2003). In this study, we observed broad distribution of the virus in the CNS with particularly high transduction rates in the cortex, hippocampus, striatum, and

thalamus. Despite a lower transduction rate (< 20% of cells transduced), expression in the cerebellum may play a role in the abnormal gait we observed as the cerebellum is significantly involved in coordination and balance. Indeed, in this model, the cerebellum significantly accumulated GlcCer (Fig. S3B), showed increased astrogliosis (Fig. 5A, C) had reduced calbindin mRNA, a marker for Purkinje neuron health (Fig. S8). Cumulatively, these findings suggest the Purkinje cells of the cerebellum may be more sensitive to perturbations in GCase activity.

The administration of AAV1-GFP-miR-*Gba* to the $Gba^{D409V/D409V}$ mouse model represents a novel neuronopathic model of GD. These mice display progressive behavioral impairments and significant CNS lipid accumulation. Importantly, this model has a delayed onset of neurological dysfunction and an extended lifespan (up to 36 weeks of age) allowing for greater flexibility for testing therapeutics. As potential therapies for types 2 and 3 GD are developed, this model may represent an important preclinical tool for proof of efficacy studies.

Supplementary data to this article can be found online at https://doi.org/10.1016/j.nbd.2019.104513.

Funding

All research was funded by Sanofi. This research did not receive any specific grant from funding agencies in the public, commercial, or not-for-profit sectors.

Acknowledgements

The authors would like to acknowledge Tatyana Taksir, John Marshall, Juanita Campos-Rivera, Jacqueline Saleh and R&D Vector Production at Sanofi including Denise Woodcock, Shelley Nass, Brenda Burnham, and Maryellen Mattingly for technical support and advice.

References

Abdelwahab, M., et al., 2017. Previously unrecognized behavioral phenotype in Gaucher disease type 3. Neurol. Genet. 3 (3), e158.
Dahl, M., et al., 2015. Lentiviral gene therapy using cellular promoters cures type 1 Gaucher disease in mice. Mol. Ther. 23 (5), 835–844.
Farfel-Becker, T., Vitner, E.B., Futerman, A.H., 2011. Animal models for Gaucher disease research. Dis. Model. Mech. 4 (6), 746–752.
Grabowski, G.A., 2008. Phenotype, diagnosis, and treatment of Gaucher's disease. Lancet 372 (9645), 1263–1271.
Hammond, S.L., et al., 2017. Cellular selectivity of AAV serotypes for gene delivery in neurons and astrocytes by neonatal intracerebroventricular injection. PLoS ONE 12 (12), e0188830.
Lentz, T.B., Gray, S.J., Samulski, R.J., 2012. Viral vectors for gene delivery to the central nervous system. Neurobiol. Dis. 48 (2), 179–188.
Machaczka, M., et al., 2018. Novel hyperkinetic dystonia-like manifestation and neurological disease course of Swedish Gaucher patients. Blood Cell Mol. Dis. 68, 86–92.
Marshall, J., et al., 2010. Improved management of lysosomal glucosylceramide levels in a mouse model of type 1 Gaucher disease using enzyme and substrate reduction therapy. J. Inherit. Metab. Dis. 33 (3), 281–289.
Marshall, J., et al., 2016. CNS-accessible inhibitor of glucosylceramide synthase for substrate reduction therapy of Neuronopathic Gaucher disease. Mol. Ther. 24 (6), 1019–1029.
Mistry, P.K., et al., 2014. Glucocerebrosidase 2 gene deletion rescues type 1 Gaucher disease. Proc. Natl. Acad. Sci. U. S. A. 111 (13), 4934–4939.
Neudorfer, O., et al., 1996. Occurrence of Parkinson's syndrome in type 1 Gaucher disease. QJM: Int. J. Med. 89 (9), 691–694.
Orvisky, E., et al., 2000. Glucosylsphingosine accumulation in mice and patients with type 2 Gaucher disease begins early in gestation. Pediatr. Res. 48, 233.
Orvisky, E., et al., 2002. Glucosylsphingosine accumulation in tissues from patients with Gaucher disease: correlation with phenotype and genotype. Mol. Genet. Metab. 76 (4), 262–270.
Passini, M.A., et al., 2003. Intraventricular brain injection of adeno-associated virus type 1 (AAV1) in neonatal mice results in complementary patterns of neuronal transduction to AAV2 and total long-term correction of storage lesions in the brains of beta-glucuronidase-deficient mice. J. Virol. 77 (12), 7034–7040.
Passini, M.A., et al., 2011. Antisense oligonucleotides delivered to the mouse CNS ameliorate symptoms of severe spinal muscular atrophy. Sci. Transl. Med. 3 (72), 72ra18.
Pinel, J., Rovner, L., 1978. Electrode placement and kindling-induced experimental epilepsy. Exp. Neurol. 58 (2), 335–346.
Rosenbloom, B., et al., 2011. The incidence of parkinsonism in patients with type 1 Gaucher disease: data from the ICGG Gaucher registry. Blood Cell Mol. Dis. 46 (1), 95–102.
Roshan Lal, T., Sidransky, E., 2017. The Spectrum of neurological manifestations associated with Gaucher disease. Diseases 5 (1), 10.
Sanders, A., et al., 2013. Transgenic mice expressing human glucocerebrosidase variants: utility for the study of Gaucher disease. Blood Cell Mol. Dis. 51 (2), 109–115.
Sardi, S.P., et al., 2011. CNS expression of glucocerebrosidase corrects alpha-synuclein pathology and memory in a mouse model of Gaucher-related synucleinopathy. Proc. Natl. Acad. Sci. U. S. A. 108 (29), 12101–12106.
Sardi, S.P., et al., 2013. Augmenting CNS glucocerebrosidase activity as a therapeutic strategy for parkinsonism and other Gaucher-related synucleinopathies. Proc. Natl. Acad. Sci. 110 (9), 3537–3542.
Shawky, R.M., Elsayed, S.M., 2016. Treatment options for patients with Gaucher disease. Egypt. J. Med. Human Genet. 17 (3), 281–285.
Snyder, E.Y., Taylor, R.M., Wolfe, J.H., 1995. Neural progenitor cell engraftment corrects lysosomal storage throughout the MRS VII mouse brain. Nature 374, 367.
Tayebi, N., et al., 2003. Gaucher disease with parkinsonian manifestations: does glucocerebrosidase deficiency contribute to a vulnerability to parkinsonism? Mol. Genet. Metab. 79 (2), 104–109.
Xu, Y.H., et al., 2003. Viable mouse models of acid beta-glucosidase deficiency: the defect in Gaucher disease. Am. J. Pathol. 163 (5), 2093–2101.